THE JOURNAL OF PHYSICAL CHEMISTRY A

Anatolian University Libraries Consortium a·n·k·o·s

Subscriber access provided by HACETTEPE UNIVERSITESI KUTUPHANESI

Article

Reaction Mechanism of 4-Chlorobiphenyl and the NO3 Radical: An Experimental and Theoretical Study

Jin Shi, Wenlong Bi, Shenmin Li, Jianmin Chen, and Wenbo Dong

J. Phys. Chem. A, **Just Accepted Manuscript** • DOI: 10.1021/acs.jpca.6b08626 • Publication Date (Web): 12 Apr 2017

Just Accepted

ACS Publications

The Journal of Physical Chemistry A is published by the American Chemical Society. 1155 Sixteenth Street N.W., Washington, DC 20036

Reaction Mechanism of 4-Chlorobiphenyl and the NO_3 Radical: An Experimental and Theoretical Study

Jin Shi†, *Wenlong Bi*†, *Shenmin Li*‡, *Wenbo Dong*†*, and *Jianmin Chen*†*

†Department of Environmental Science and Engineering, Fudan University, Shanghai, 200433, P. R.China.

‡College of Environmental and Chemical Engineering, Dalian University, Dalian, 116622, P.R.China.

ABSTRACT: An experiment and theoretical chemistry calculation were conducted to elucidate the mechanism of the reaction between 4-chlorobiphenyl (4-CB) and the NO_3 radical. The degradation of PCBs was investigated mechanistically through transient absorption spectroscopy technology and high-accuracy theoretical calculation byusing 4-CB as the model. Laser flash photolysis (LFP) experiments were performed at 355 nm. The main intermediate was analyzed through transient absorption spectroscopy and identified to be a charge transfer complex (CTC). The final products were identified through GC-MS analysis. The ground states and excited states of the reactants were calculated through density functional theory (DFT) method. The absorption bands at 400 and 700 nm show good agreement with the experimental results. The ratio of absorbance at 400 and 700 nm is 1.6, and the experimental value is 1.8. Analysis of the charge population, indicated that one unit charge transfer from 4-CB to NO_3. The entire reaction process was divided into two phases. In the first phase, the CTC intermediate was formed by electrostatic attraction between 4-CB and the NO_3 radical. In the second phase, the

most important channel of subsequent reactions is the σ-complex as intermediate formed as an intermediate by N-C coupling. The final product 4-chloro,2-nitrobiphenyl was generated with the breakage of $B_{C\text{-}H}$ and $B_{N\text{-}O}$, and benzene derivatives were formed by other channels.

INTRODUCTION

Polychlorinated biphenyls(PCBs) are dangerous persistent organic pollutants (POPs) in the environment. PCBs can enter the body through respiration and accumulate when organisms, such as humans and animals, are exposed to PCB-contaminated surroundings[1-4]. PCBs also pose carcinogenic, teratogenic, and mutagenic threats on the physical health of humans and animals. PCBs are detected in oceans, soil, and the atmosphere, though banned from production for numerous years. Thus, PCB remaines as a serious worldwide environmental problem worldwide [5]. Photolysis is an important decomposition pathway of PCB in the environment. Photochemical processes based on free radicals have been extensively investigated and applied. PCBs can be stimulated by various radicals, such as OH, HO_2, NO_3, and O_3, under natural conditions. The OH radical initiates a chain reaction in the daytime, whereas the NO_3 radical exhibits high reaction activity at night. The oxidation of hydrocarbon, which is initiated by the NO_3 radical, constitutes a significant nighttime loss process[6]. The concentration of the NO_3 radical is also higher than that of the OH radical at night [7, 8]. The NO_3 radical is another

key free radical that can trigger various free radical reactions and plays an important role in degradation of organic pollutants in the atmosphere and condensed phase [8-16]. Mechanistic studies of these reactions with naphthalene, pinene, and alkene revealed that the NO_3 addition initiates a degradation process, which leads to the formation of oxygenated organic products. The NO_3 radical has received increasing research attention. However, the precise degradation mechanism of PCBs remains unclear, and limited information is available regarding the mechanism of PCB reactions initiated by the NO_3 radical.

Laser flash photolysis (LFP) is an efficient technique used to investigate reaction mechanisms[17-21], including charge transfer. Quantum chemical calculation can also provide a safe and accurate alternative to examine highly toxic compounds. In recent years, research of PCBs by using DFT yielded satisfactory results[22-26]. In this paper, we selected 4-CB as research object with a single *para* chlorine substituent. The reaction mechanism involving 4-CB and the NO_3 radical was investigated through LFP and theoretical calculation. This study provides a basis for degradation of PCBs and other POPs with NO_3 radical.

EXPERIMENTAL SECTION

Reagents Analytical-grade 4-CB (>99.4%, Sigma-Aldrich), fumaronitrile (>98%, ACROS), ceric ammonium nitrate (CAN. Shanghai Chemical Reagent Co.), and acetonitrile (>99.8%, high-performance liquid chromatography (HPLC) eluent, Shanghai Ling-feng Chemical Reagent Co.) were used without further purification. The mixed reaction solution of 4-CB and CAN was diluted to 1.0×10^{-4} mol·L^{-1} in acetonitrile solution.

LFP Experiments Photolysis experiments were carried out in 1 cm × 1 cm quartz cuvettes. Reaction solutions were deoxygenated by bubbling in high-purity nitrogen. A nanosecond LFP apparatus was used as described in detail in a previous work [27]. A 355 nm laser beam was used as excitation source for all LFP experiments and provided by third harmonic radiation from a Quanta-Ray LAB150 Nr-YAG laser (Applied Photophysics Ltd.). The full width at half maximum (FWHM) of the laser pulse was 10 ns. Laser intensity was detected with five-stage (R928) and nine-stage (1P28) photomultiplier tube detectors. The absorption intensities of transients were obtained in a point-by-point manner at the corresponding wavelengths [19]. A Xenon lamp (XBO 150W/CR-OFR, OSRAM GmbH.) was used as an analyzing light source. A filter was applied to cut off the band of the analyzing light below 450 nm so as to prevent

excitement induced by the analyzing light and to obtain the transient spectra above 450 nm. The reaction samples were renewed immediately after irradiation to prevent secondary photolysis. Furthermore, the rate constant of the reaction was fitted by using Pro-Kinetics (Applied Photophysics Ltd.).

Acetonitrile was used as solvent in the LFPs. During our investigations, we tested and checked numerous of solvents, including cyclohexane and water. For water, CAN can be dissociated in aqueous solution. Especially for cyclohexane, cyclohexane is a good non-polar solvent, but this solvent is inappropriate. Atkinson[2] reported that the rate constant of the reaction between the NO_3 radical and cyclohexane is 2.4×10^4 $L\bullet mol^{-1}\bullet s^{-1}$. In our experiments, we discovered that the decay rate coefficient of NO_3 radical is 3.76×10^5 $L\bullet mol^{-1}\bullet s^{-1}$, whereas the oxidation and autoxidation of cyclohexane can be photochemically promoted by CAN[29]. To minimize side reaction, we did not select cyclohexane as solvent, instead, we selected acetonitrile mainly because the production process of NO_3 radical is a mature technology in acetonitrile solvent. In this technology, the photolysis of CAN can lead to the formation of the NO_3 radical in acetonitrile. Therefore, acetonitrile was selected as the solvent in our LFP experiments.

Generation of the NO_3 Radical Strong evidence vidence demonstrating NO_3 free radical generation through CAN photolysis was provided by Glass et al. [30-34]. In our research, the NO_3 radical was obtained through LFP of 1.5×10^{-4} $mol\cdot L^{-1}$ CAN solution at 355 nm. The formation of the NO_3 radical involves the charge transfer of an

intramolecular excited state, as described in the following reaction scheme:

$$\left[\left(NH_4\right)_2 Ce^{IV}\left(NO_3\right)_6\right] \xrightarrow[MeCN]{h\nu} \left(NH_4\right)_2 Ce^{IV}\left(NO_3\right)_6^* \quad (1)$$

$$\longrightarrow \left(NH_4\right)_2 Ce^{III}\left(NO_3\right)_5 + NO_3 \quad (2)$$

The transient absorption spectrum of NO_3 is presented in Figure 1 and obtained through the following procedures. (i) Negative absorption was corrected in the region between 280 and 450 nm. A negative absorption signal results from the absorption within the range of 280–450 nm and the decomposition of CAN [27]. (ii) The transient spectrum of NO_3 at 1.9 μs was identified in the region between 450 and 700 nm, with three peaks at 590, 630, and 670 nm [35]. The extinction coefficient of the NO_3 radical was calculated as 1290 $L \cdot mol^{-1} \cdot cm^{-1}$ at 630 nm, and this value closely approximates the value in to Giacco's work [32].

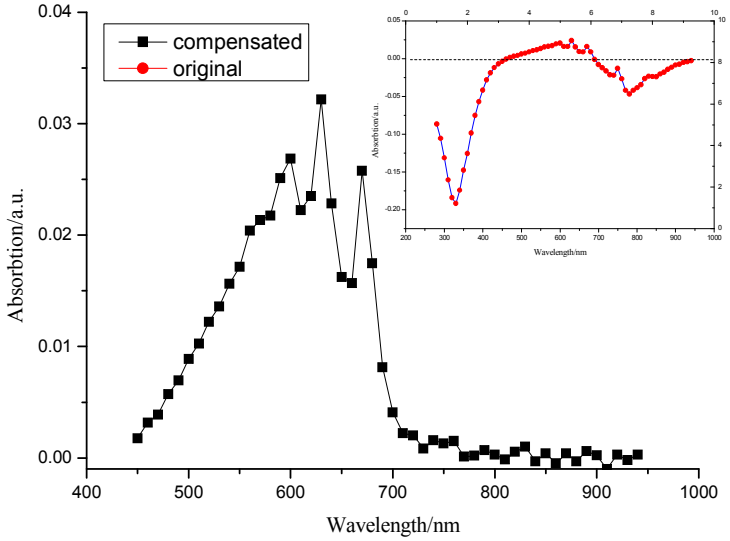

Figure 1. Transient absorption spectra of the laser flash photolysis (LFP) of NO_3 in acetonitrile at 1.9 μs. Inset: transient absorption spectra of the LFP of CAN in acetonitrile.

Final Product Analysis The reaction mixture (120 mL) was separated into 40 equal parts, and each equal part of the reaction solution was irradiated by the laser beam in 10 Hz mode for 5 s, that is, 50 pulses, with 10 mJ for each pulse. The position of the cuvette was continuously adjusted to decrease the overlap of irradiation spots and reduce the likelihood of a secondary photolysis reaction. Afterward, the reaction solution was bubbled with pure nitrogen to remove acetonitrile and then dissolved in 30 mL of water. Organic phases were extracted several times by using 30 mL of CH_2Cl_2, and CAN was maintained in the aqueous phase. The final organic products were detected through gas chromatography-mass spectroscopy (GC-MS, 6890A/5975C, Agilent, USA) and HPLC (UltiMate 3000, Dionex, USA).

COMPUTATIONAL DETAILS

Theoretical calculations were carried out in Gaussian 09 [36]. DFT method with a standard split valence basis set of 6-311+G(d,p) can provide a good compromise between calculation time and the quality of the result. The geometrical structures of reactants, transition states (TSs), intermediates, and products were optimized at the same basis set level with the IEFPCM solvent model. Charge population was calculated with five models, including Mulliken population analysis, Charges from Electrostatic Potentials (CHelp) population analysis, Charges from Electrostatic Potentials using a Grid-based method (CHelpG) population analysis, Merz−Kollman (MK) population analysis, and natural population analysis (NPA). The UV-vis spectrum of the excited state was obtained via a linear response time−dependent DFT method[37,38]. All open-shell species were described with an unrestricted approach, whereas closed-shell species were explained with a restricted method. The single-point energy of the involved species was calculated at the level of second-order Møller−Plesset perturbation theory[39]. Furthermore, the thermochemistry properties of chemical reactions were investigated through vibrational frequency calculations, which were also applied to characterize the stationary point. Besides, given the solvent effect, all projects were computed at the same basis set level with gas phase (see Supporting Information).

The numbering scheme for the main carbon atoms of 4-CB is shown in Figure 2. 4-CB is characterized by two conformational isomers with a dihedral angle ($D_{2\text{-}1\text{-}1'\text{-}2'}$) of ±38.67° because of the dual influences of the inductive effect and the conjugative effect. However, the energy of both isomers could be optimized to the same local minimum. Therefore, a stable structure with −38.67° was randomly selected as a model. The NO_3 free radical likely attacks the low-stereo-hindrance position of the reactant.

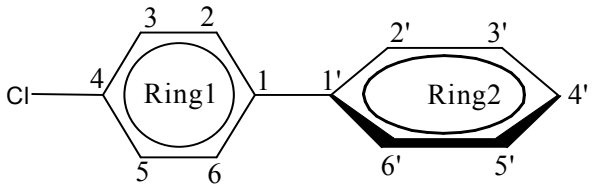

Figure 2. Numbering scheme for the main carbon atoms of 4-CB.

The bridge bond carbons (C1 and C1′) of 4-CB could not be easily attacked by the NO_3 free radical because of the absence of H atom and high steric hindrance. Although C4 position is occupied by a highly electronegative Cl atom, the electron-deficient NO_3 radical would also be attracted by the Cl atom with high electron density. Thus, the C4 position is a potential site for reaction. Owing to structural symmetry, the C5, C6, C5′, C6′ positions are equivalent to C3, C2, C3′, and C2′ positions, respectively. Therefore, six positions of 4-CB, namely, C2, C3, C4, C2′, C3′, and C4′, was considered and investigated in the theoretical calculation. Potential barrier (E*), vibrational frequency (f), UV-vis absorption spectrum, and charge population were also determined in this work.

RESULTS AND DISCUSSION

Experiments

Transient absorption spectrum The transient absorption spectrum of LFP provides good insight into the reaction mechanism involving 4-CB and the NO_3 free radical. The negative absorption signal in the range of 280–450 nm could be compensated when the consumption of CAN was considered. The transient absorption spectra of the reactions are displayed in the inset of Figure 3.

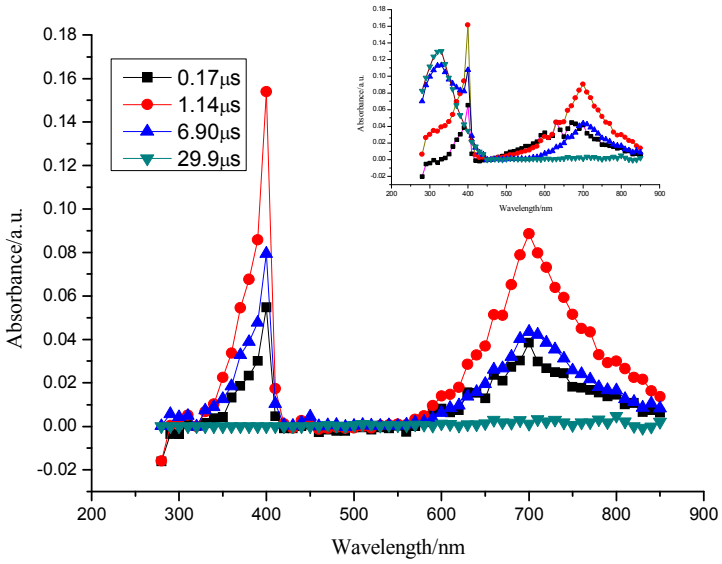

Figure 3. Time-resolved transient spectrum of intermediate(s) recorded at 0.17 μs. Inset: Time-resolved transient spectrum of the reaction recorded at 0.17 (■), 1.14 (●), 6.90 (▲), and 29.9 μs (▲).

The time-resolved transient spectra of the reactions were obtained at 0.17, 1.14, 6.90, and 29.9 μs. Three evident peaks appeared in the region of 280–850 nm (inset of Figure 3). The three peaks at 320, 400, and 700 nm could be assigned to different species. In the 280–450 nm region, the maximum absorption peak of this species appeared at 320 nm and grew with time; thus, the absorption peak corresponds to the final product. The absorption spectra of the transient species could be obtained by subtracting the absorption of the final product and the NO_3 radical from the time-resolved transient spectra (Figure 3). The absorption peaks at 400 and 700 nm were assigned to the characteristic absorption bands of the transient state(s). A high correlation between the absorbance values of two peaks at 400 and 700 nm indicate that the peaks could be assigned to the same transient species. Several possible reaction mechanisms were fitted in Pro-K. The kinetics and the absorption spectra of various species were obtained. Our results suggest that the most probable reaction mechanism could be expressed in Eqs. (3) and (4):

$$\text{4-CB(280nm)}+\text{NO}_3 \xrightarrow{k_2} \text{I(400nm,700nm)} \quad (3)$$

$$\text{I(400nm,700nm)} \xrightarrow{k_3} \text{P} \quad (4)$$

where *I* and *P* represent the intermediate product and the final product, respectively. The fitting result also indicates that a second-order reaction could occur between 4-CB and the NO_3 radical, and the rate constant k_2 was $6.90\pm0.08\times10^9$ $L\cdot mol^{-1}\cdot s^{-1}$. The first-order decay rate constant k_3 of *I* was $1.47\pm0.05\times10^5$ s^{-1}. The characteristic absorption of *I* was

detected at 400 and 700 nm. Comparing the spectra of *I* and 4-CB cation (4-CB^+), we found that their characteristic absorption wavelengths were completely consistent at 400 and 700 nm. However, the ratio of the absorbance values of *I* at 400 and 700 nm was 1.8, which was considerably lower than that of 4-CB^+ (2.8). Therefore, the transient species was possibly a charge transfer complex (CTC), which may exhibit an extinction property similar to that of 4-CB^+.

Analysis of the final products The final products of LFP were obtained through GC-MS (Figure 4) and categorized as follows: (a) nitro-compound (retention time: 11.698, 12.731, and 13.618 min), which may be the main product of the reaction between 4-CB and the NO_3 radical; (b) chlorinated biphenyl compounds with other substituent groups, such as chlorinated diphenol (retention time: 13.538 min); (c) benzene derivatives, which may be produced through ring opening or bridge bond cleavage, with retention times of less than 9 min; (d) complicated compounds, including dibenzofuran (retention time: 14.465 min). On the basis of final product analysis, we observed that the reaction of 4-CB with the NO_3 radical is extremely complicated, thus, the formation pathways of these products could not be easily understood. Moreover, the lifetime of several transient species was too short to be captured by the LFP spectrum. To resolve this drawback and interpret the reaction mechanism, we performed a theoretical calculation to study the nitrated mechanism of 4-CB. In this work, we proposed the possible reaction pathway, which was determined at the (U)B3LYP/6-311+G(d,p) level.

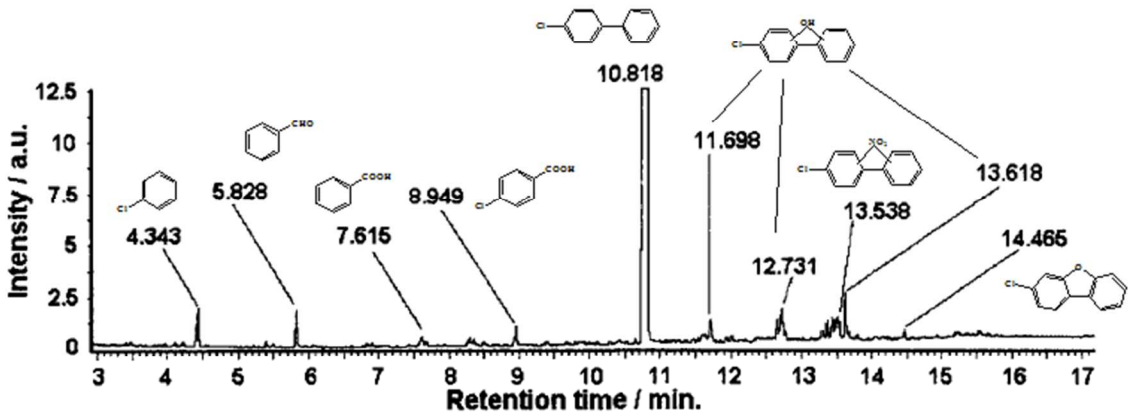

Figure 4. Gas chromatogram of the solution extracted with CH_2Cl_2 of 4-CB in CAN−acetonitrile after 5 s of irradiation with 355 nm laser.

Theoretical calculations

Identification of intermediate The energy minimized molecular geometries of the isolated the 4-CB, NO_3 free radical, and the 4-CB⋯NO_3 complex were determined at the (U)B3LYP/6-311+G(d,p) level, and the solvent effect was included through the IEFPCM model [40]. Two very probable pathways of the reaction between 4-CB and the NO_3 radical are illustrated in Scheme 1. Pathway *a* can be described as a NO_3 addition reaction, and the transition state is an σ-complex formed by C-N coupling. Pathway *b* is a process of H-O interaction, and the formation of the transition state begins with a mutual attraction between oxygen and hydrogen.

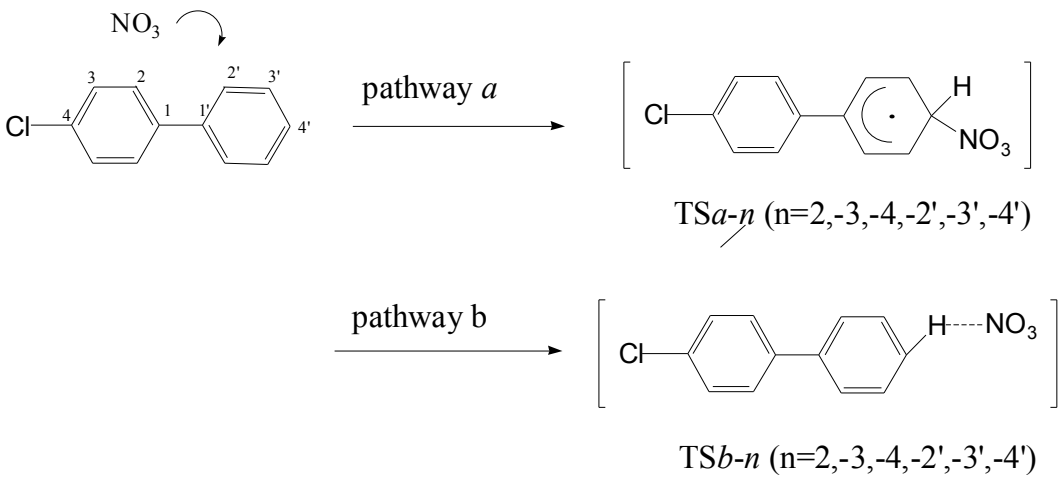

Scheme 1: Pathway *a*: The transition state is an *σ*-complex formed by C-N coupling.

Pathway *b*: The transition state was a H−O coupling complex.

n: the sequence number of a carbon atom.

Table 1. Potential barrier *E** (kcal/mol), and imaginary frequency *f* (*i*cm^{-1})

		4′	3′	2′	2	3	4
*E**	TS*a*	101.055	103.323	105.882	109.386	110.831	--
	TS*b*	24.204	24.103	30.953	24.650	24.650	--
f	TS*a*	1440.32	1281.80	1383.61	1360.00	1329.72	--
	TS*b*	3207.76	3206.43	2082.27	2066.96	765.31	--

The transition states on the C4 position was not found probably because of the extremely high energy barrier. Besides, Table 1 shows that one imaginary component was found through the vibrational frequency calculation of the transition state. The reaction potential barrier *E** of Pathway *a* is higher than that of Pathway *b*. Therefore, Pathway 2 is the thermodynamically favorable process. Moreover, we calculated these parameters in the gas phase, and the results are shown in Table S1 and Table S2. We found that the vibration mode and value of transient state are the same as the situation with that of the acetonitrile solvent. Based on their relative energy, the stability of the intermediates is the same, and CTC2′ is the most stable intermediate structure.

We also determined whether charge transfer occurs from 4-CB to NO_3 on TS*b*. Six CTC intermediates, namely, CTC2, CTC3, CTC4, CTC2′, CTC3′, and CTC4′, were built as H···O structures (or Cl···O) and optimized at the same level. Relative energy, charge population, and excited state spectrum were analyzed to identify and confirm the possible transient species.

The six complexes were isomers of one another, thus, their similar characteristic absorption bands are difficult to understood (Table 2). The absorption peak wavelengths λ around 350 and 650 nm corresponded to 400 and 700 nm in the experiments, respectively. The ratio of A350 nm/A650 nm was approximately 1.6, which was closer to the ratio of 1.8 obtained through experimental analysis. The probable intermediate may be a complex structure of NO_3 and 4−CB, and the complex was formed under the

electrostatic attraction; hence, the intermediate is a type of CTC.

Table 2. E/kcal•mol^{-1}, λ/nm, T, and ratio of six CTCs.

TSb	CTC4′	CTC3′	CTC2′	CTC2	CTC3	CTC4
E	1.11	0.31	0.00	0.0075	0.81	1.41
Λ	652.32, 350.58	626.27, 354.300	643.26, 350.09	630.73, 353.35	648.53, 351.08	655.25, 352.54
$\boldsymbol{T}$	0.314, 0.530	0.294, 0.4690	0.301, 0.497	0.294, 0.460	0.312, 0.524	0.3219, 0.504
Ratio	1.688	1.595	1.651	1.528	1.679	1.5657

To order to locate the most probable intermediate configuration, we first analyzed the population charge data of 4-CB supply helpful information. The population charge of 4-CB was computed by several models [41-43] and displayed in Table 3: (a) CHelp, CHelpG, and MK population analyses and (b) NPA. For Mulliken analysis, the equal division of the off-diagonal terms between the two basis-functions leads to exaggeration in the charge separation in molecules. Furthermore, Mulliken charge is sensitive to the basis set choice[43]. However, several modern methods were explored to calculate net atomic charges. For CHelp, CHelpG, and MK methods, atomic charges are fitted to reproduce

the molecular electrostatic potential at a number of points around a molecule [41]. In the NPA method, atomic charges are obtained by calculating the electron density distribution in atoms. The problems of the Mulliken method could be addressed by modern methods; thus, CHelp, CHelpG, MK, and NPA were more credible than Mulliken method. As an electron-withdrawing group, Cl presents a slightly negative charge. The *p*-electron of Cl may participate in delocalized π bonding of the aromatic ring. In other words, the conjugation effect could stabilize the structure of 4-CB. From Table 3, we analyzed the total charge of each benzene ring (Ring 1 and Ring 2) and found that Ring 1 (chlorobenzene) presents a slightly negative charge and Ring 2 (benzene) contains an equivalent positive charge. Thus, Ring 1 can act as an electro-donating substituent. Moreover, we examined the population charge of each C atom and observed that C2′ and C4′ positions are slightly negatively charged. Thereby, the NO_3 radical preferentially attacks C2′ and C4′ positions. Therefore, based on this analysis, C2′ and C4′ are high reactivity positions. Theoretically, the -Cl group could affect the reactive site distribution of 4-CB. The –Cl group withdraws electrons by inductive effect (-I effect). However, this group also releases electrons by delocalization of lone pairs (+R effect). By contrast, the inductive effect is stronger than the resonance effect in case of halogen atoms. As a result, the electron density decreases in both of benzene rings, and negative charge is mainly concentrated on −Cl group. The electron density of R1 is less than that of R2. Meanwhile, the NO_3 radical is an electron-deficient group is thus directed at the *ortho* and *para* positions of R1, namely, C2′ and C4′ positions, instead of the *meta*- position. This result

is consistent with charge population analysis. In addition, the charge population of 4-CB were analyzed in the gas phase (in Table S3) and consistent with the charge population of the acetonitrile solvent.

Based on the calculation of relative energy, CTC2′ is the most thermodynamically stable structure with the lowest relative energy (see Table 2). Moreover, we examined the structure of six CTCs; as displayed in Figure 5, only CTC2′ behaved as a nearly planar structure. The structure displays that two O atoms in NO_3 interact with two H atoms linking C2 and C2′ in 4-CB; thus, four hydrogen-bond-like structures were formed in CTC2′. These O⋯H weak interactions caused the decreased in the dihedral angle *D*(2-1-1′-2′) to −16.54°, thus, the resistance of the electron flow was decreased between two benzene rings and the charge could flow easily on this structure. Moreover, the complex was stabilized by the delocalization of electrons. Hence, the reactivity of C2′ position is higher than that of C4′ position. In addition, according to the symmetry of the molecule, the reactivity of C6′ position is equivalent to that of C2′. As a result, C2′ (C6′) position is attacked with more probability compared with the C4′ position. CTC2′ is the optimal intermediate in this process.

Table 3. Population charge of 4-CB.

	Chelp	ChelpG	MK	NPA
C1	−0.337	0.031	0.077	−0.054
C2	0.089	−0.123	−0.211	−0.177
C3	0.042	−0.092	−0.065	−0.226
C4	−0.110	0.105	0.007	−0.041
C1′	0.044	0.057	0.087	−0.060
C2′	−0.035	−0.119	−0.173	−0.197
C3′	0.084	−0.099	−0.137	−0.204
C4′	−0.249	−0.080	−0.142	−0.212
Cl	-0.101	-0.181	-0.140	-0.017
Ring 1	−0.114	−0.021	−0.022	−0.009
Ring 2	0.114	0.021	0.022	0.009

Note: C1 indicates that the sequence number of carbon is 1.

However, other conformation isomers could be considered as possible intermediates.

These isomers probably appeared in the initial formation phase of the intermediate and then isomerized into a more stable structure. As evident from the above data, C2′ position is the optimum nucleophilic site, and CTC2′ is the optimum potential intermediate conformation in the process. This speculation are in good agreement with the literature[26]. In summary, the optimal intermediate in this process is CTC2′, which is estimated by analyzing the relative energies, charge population, and excited state spectrum.

For further study of the subsequent reactions, the charge population of CTC2′ was computed at the same level as shown in Table 4. Two findings were obtained: (1) the net charge value of the NO_3 radical is approximately equal to −1, that is, NO_3 and 4-CB respectively act as a charge acceptor and a charge donor; (2) 1*e* can be transferred from the delocalized π-bonding orbitals of 4-CB to the NO_3 radical. Table 3 also shows that the transferred charge is donated by both Ring 1 and Ring 2. In addition, the charge may be directly transferred from Ring 1 and Ring 2. Another possibility is that a partial charge flow occurred from Ring 1 to Ring 2 or vice versa, and 1*e* was transferred from Ring 2 or Ring 1 to the NO_3 radical. The phase of the reaction pathway can be summarized as follows: $A + D \xrightarrow{h\nu} A + D^* \longrightarrow A\ldots\ldots D^* \xrightarrow{\text{ct}} A^+\ldots D^-$. The calculation results of gas phase are shown in Table S4. The only difference is that the CTC2′ exhibits a charge transfer character with approximately 0.5 charge transferred to the NO_3 radical.

Table 4. Population charge of CTC2′. Charge transfer value (q) under CHelp, CHelpG, MK, and NPA models.

	Chelp	ChelpG	MK	NPA
C1	−0.069	0.106	0.149	0.021
C2	−0.070	−0.099	−0.178	−0.124
C3	0.0064	−0.061	0.0145	−0.205
C4	0.245	0.180	0.040	0.041
C1′	0.281	0.078	0.148	0.000
C2′	−0.167	−0.082	−0.127	−0.130
C3′	0.025	−0.087	−0.126	−0.196
C4′	−0.081	0.071	0.028	−0.067
O	−0.730	−0.704	−0.695	−0.557
N	1.287	1.165	1.084	0.693
O	−0.677	−0.705	−0.691	−0.558
O	−0.806	−0.712	−0.680	−0.544

Ring 1	0.502	0.507	0.468	0.546
Ring 2	0.487	0.460	0.498	0.441
Q	−0.989	−0.967	−0.966	−0.988

Formation mechanism of final products As shown in Table 4, the C2 and C2′ positions of CTC2′ contain a slight negative charge, while N atom possesses a partial positive charge. Moreover, the total atomic charge of Ring 1 is negative. Therefore, N atom tends to localize on C2 position. The rearrangement of CTC2′ is the probable channel in the subsequent reaction. The σ-complex as a new intermediate was formed during this process, accompanied by along with the elongation of one *B*(N-O) and *B*(C2′-H) and the shortening of *B*(O-H). In this channel, 4-chloro,2-nitrobiphenyl was formed by the breakage of *B*(C2′-H) and *B*(N-O) accompanying the formation of OH radical (see Figure 5). The theoretical calculation of the excited state spectrum reveals that the maximum absorption peak of 4-chloro,2-nitrobiphenyl is at 252.36 nm, which corresponds to 320 nm of the LFP experiments. The error could be attributed to systematic error, which was found to be at the same level as that of intermediates. Therefore, these properties indicate that 4-chloro,2-nitrobiphenyl was the main final product in this pathway.

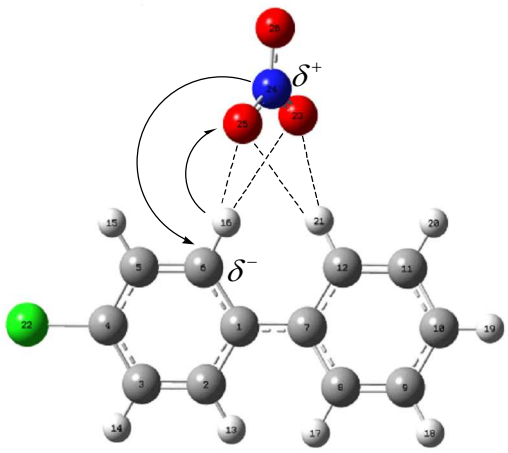

Figure 5. Schematic of the re-arrangement of CTC2′.

As shown in Figure 4, numerous of final products were found, whereas chlorinated nitrobiphenyl is absent. This finding suggestes that reaction pathway proceeded in the second phase. First, we checked the structure parameters of CTC2′ because of electron redistribution in the intermediate. Not only dihedral angles but also several bond lengths varied to a certain extent. *R*(C1-C1′) and *R*(C4-Cl) were slightly shortened by 0.044 and 0.041 Å, respectively. *R*(C1-C2) and *R*(C1′-C2′) were elongated by approximately 0.025 Å because of the weak hydrogen bond (O⋯H) interactions. Furthermore, the population charges of C1 and C1′ decreased to similar levels (see Tables 3 and Table 4). These findings suggest that the polarity of bond *B*(C1-C1′) was enhanced and that the breakage of the bridge bond was accelerated. After the generation of 4-chloro,2-nitrobiphenyl, the electrons are displaced in the direction of the $-NO_2$ group. On one hand, $-NO_2$ group is more electronegative than the –Cl group. On the other hand, the $^{-}NO_2$ group withdraws

electrons by delocalizing lone pairs (-R effect). Thus, the electron density increases on the C1 position, and the reactivity towards electrophilic substitution increases on C1 position. Except for the pathway of 4-chloro,2-nitrobiphenyl, other possible subsequence reaction channels existed in this pathway. We also noticed that the OH radical is generated with the formation of chlorinated nitrobiphenyl. Owing to a small size, the OH radical may attack bridge-bonding carbons, which cleave the bridge bond *B*(C1-C1′). Moreover, we studied the reactions of the OH radical attacking the C1/C1′ positions. The two reactions were exothermic by about 3.0 kcal/mol with the low limit below 15.0 kcal/mol. In consequence, the breakage of the bridge bond and open-ring are suggested to be the probable reaction channels. Thus, several benzene derivatives, such as chlorobenzene (retention time: 4.343 min), benzaldehyde (retention time: 5.828 min), benzoic acid (retention time: 7.615 min), and *p*-chlorobenzoic-acid (retention time: 8.949 min), may be generated in the subsequent reaction.

Three chlorinated diphenols are displayed in Figure 4. Evidently, the three chlorinated diphenols are the products of hydroxy addition reaction. For 4-CB, benzene and chlorobenzene groups are *ortho*–*para*–direction groups. The 2-, 2′-, 4′- substitutions were subject to OH radical attack in this process, thus resulting in the formation of the three chlorinated diphenols.

In addition, we noticed that a small quantity of chlorinated dibenzofuran (retention time: 14.465 min) was generated in this experiment. Presumably, chlorinated

dibenzofuran is generated from the precursor 2,2′-dihydroxy,4-chlorobiphenyl or 2-hydroxy,4-chlorine, 2′-nitrobiphenyl. The formation pathways of chlorinated dibenzofuran are depicted in Figure 6. The reliability of the transition states was further verified by Intrinsic Reaction Coordinate calculations. Only one imaginary component was acquired through calculating the vibrational frequency of the transition state. The barrier energy of Step 1 was much less than that of Step 2, therefore, Step 2a/2b is the rate-limiting step in the two probable pathways. Step 2b is an elementary reaction involving the formation of H_2O, whereas Step 2a involves two important elementary reactions, namely, the conformational isomerization of hydroxyl and the formation of chlorinated dibenzofuran and nitrous acid.

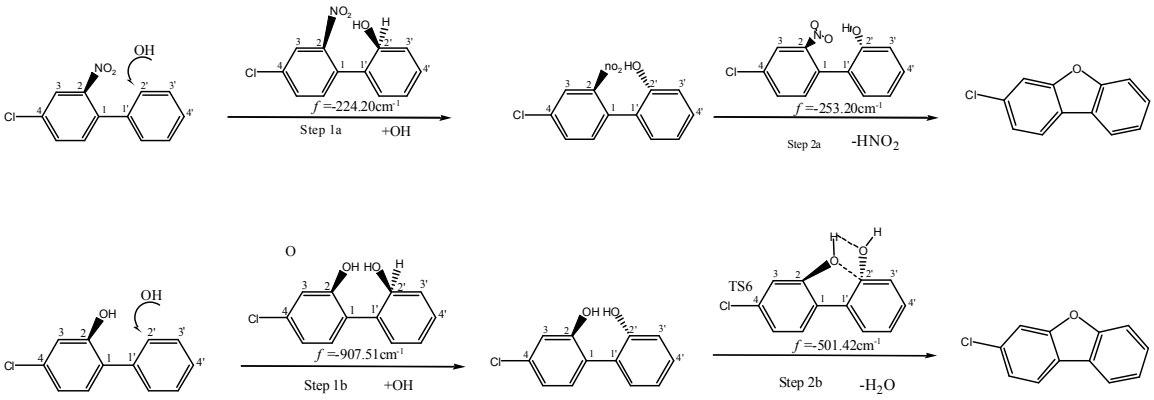

Figure 6. Probable formation pathway of chlorinated dibenzofuran

Notably, the structure of CTC4 is the least stable because of its highest electron energy. Furthermore, we carefully checked the charge population of CTC4 and found that the C4 and N atom exhibit a partially positive charge. Thereupon, we inferred that CTC4

may revert back to 4-CB and the NO_3 radical during the reaction process or rearrange into other isomers in another channel, such as CTC2′. In addition, the Cl atom returns to its original conformation in this channel. This speculation is supported by evidence stating that the dechlorination products of 4-CB are not detected experimentally by GC-MS.

CONCLUSION

The reaction between 4-CB and NO_3 free radicals was investigated in detail through a combination of LFP and theoretical calculation. This study aimed to understand relevant intermolecular interactions and the possible relationship with charge transfer between two species. Theoretical calculation data was not only in a good agreement with the result of experiments, but also described the reaction pathway in detail. In conclusion, this reaction process involves two phases. In the first phase, the charge transfer complex (CTC) intermediate was formed by the electrostatic attraction between 4-CB and the NO_3 radical. In the subsequent reactions, several reaction channels proceed in the second phase. One important channel is the formation of σ-complex as intermediate by N-C coupling. The final product 4-chloro,2-nitrobiphenyl is generated by the breakage of $B_{C\text{-}H}$ and $B_{N\text{-}O}$. Benzene derivatives, three chlorinated diphenols and chlorinated dibenzofuran were formed by other channels of the second phase. This work is also the first to perform

an extensive analysis on charge transfer involving 4-CB as an electron donor and the NO_3 radical as an electron acceptor. Theoretical computation provides new insight and computational results can accurately estimate the reactivity site. This study can be used as a basis for further studies on reactions between PCBs and free radicals. Our future efforts in this area will focus on extending the study of the reactivity site to other types of pollutants.

AUTHOR INFORMATION

Corresponding Author

*Phone: +86-65642030; e-mail: wbdong@fudan.edu.cn

Notes

The authors declare no competing financial interest.

ACKNOWLEDGMENTS

This work was supported financially by the National Natural Science Foundation of China, project No.21077027, 20777012, and China Scholarship Council, project No.201306100068.

423

424 TOC/Abstract Art

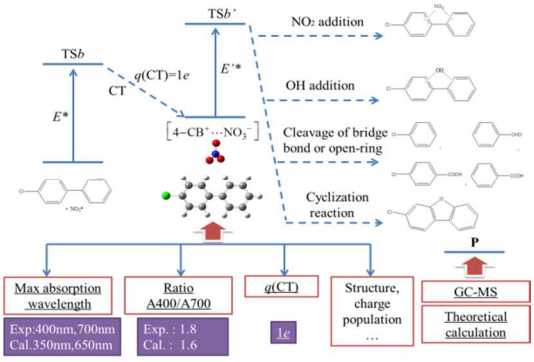

425

426

427

REFERENCES

1. Giesy, J. P.; Kannan, K. Dioxin-like and Non-dioxin-like Toxic Effects of Polychlorinated Biphenyls (PCBs): Implications for Risk Assessment. *Crit Rev Toxicol*. **1998,** *28*, (6), 511-569.
2. Van den Berg, M.; Birnbaum, L.; Bosveld, A. T. C.; Brunstrom, B.; Cook, P.; Feeley, M.; Giesy, J. P.; Hanberg, A.; Hasegawa, R.; Kennedy, S. W. et al. Toxic Equivalency Factors (TEFs) for PCBs, PCDDs, PCDFs for Humans and Wildlife. *Environ. Health. Persp*. **1998,** *106*, (12), 775-792.
3. Adams, R. G.; Lohmann, R.; Fernandez, L. A.; Macfarlane, J. K.; Gschwend, P. M. Polyethylene devices: Passive Samplers for Measuring Dissolved Hydrophobic Organic Compounds in Aquatic Environments. *Environ. Sci. Technol*. **2007,** *41*, (4), 1317-1323.
4. Osius, N.; Karmaus, W.; Kruse, H.; Witten, J. Exposure to Polychlorinated Biphenyls and Levels of Thyroid Hormones in Children. *Environ. Health. Persp*. **1999,** *107*, (10), 843-849.
5. Lohmann, R.; Breivik, K.; Dachs, J.; Muir, D. Global fate of POPs: Current and Future Research Directions. *Environ. Pollut*. **2007,** *150*, (1), 150-65.
6. Wangberg, I. B.; Becker, K.H. Product and Mechanistic Study of the Reaction of NO_3 Radicals with r-Pinene. *Environ. Sci. Technol.* **1997,** *31*, 2130-2135.
7. McLaren, R.; Salmon, R. A.; Liggio, J.; Hayden, K. L.; Anlauf, K. G.; Leaitch, W. R. Nighttime Chemistry at A Rural Site in yhe Lower Fraser Valley. *Atmos. Environ*. **2004,** *38*, (34), 5837-5848.
8. Noxon, J. F.; Norton, R. B.; Marovich, E. NO_3 In the Troposphere. *Geophys. Res. Lett*. **1980,** *7*, (2), 125-128.
9. Warneck, P. Natural Atmospheric Chemistry. **2000**.
10. Exner, M.; Herrmann, H.; Zellner, R. Laser-based Studies of Reactions of the Nitrate Radical in Aqueous-solution. *Berichte Der Bunsen-Gesellschaft- Phys Chem Chem Phys*. **1992,** *96*, (3), 470-477.
11. Wayne, R. P.; Barnes, I.; Biggs, P.; Burrows, J. P.; Canosamas, C. E.; Hjorth, J.; Lebras, G.; Moortgat, G. K.; Perner, D.; Poulet, G. et al. The Nirate Radical-physics, Chemistry, and the Atmosphere. *Atmos. Environ Part a-General Topics*. **1991,** *25*, (1), 1-203.
12. Huang, Z.; Zhang, Q.; Wang, W. Mechanical and Kinetic Study on Gas-phase Formation of Dinitro-naphthalene From 1- and 2-nitronaphthalene. *Chemosphere*. **2016,** *156*, 101-10.
13. Ye, C.; Gao, H.; Zhang, N.; Zhou, X. Photolysis of Nitric Acid and Nitrate on Natural and Artificial Surfaces. *Environ. Sci. Technol.*. **2016,** *50*, (7), 3530-6.
14. Liu, C.; Zhang, P.; Yang, B.; Wang, Y.; Shu, J. Kinetic Studies of Heterogeneous Reactions of Polycyclic Aromatic Hydrocarbon Aerosols with NO(3) Radicals. *Environ. Sci. Technol.* **2012,** *46*, (14), 7575-80.
15. Jennifer, S.; Sara, M. A.; Eric, S. C. K.; Roger, A.; Janet, A. Products of the Gas-Phase OH and NO_3 Radical-Initiated Reactions of Naphthalene. *Environ. Sci. Technol*. **1997,** *31*, 3173-3179.
16. Nguyen, T. L.; Park, J.; Lee, K.; Song, K.; Barker, J. R. Mechanism and Kinetics of the Reaction NO_3 + C_2H_4. *J Phys Chem. A*. **2011,** *115*, (19), 4894-901.
17. Zhao, S.; Ma, H.; Wang, M.; Cao, C.; Xiong, J.; Xu, Y.; Yao, S. D. Study on the Mechanism of Photo-degradation of p-nitrophenol Exposed to 254nm UV Light. *J Hazard Mater*. **2010,** *180*, (1-3), 86-90.
18. Tsao, M. L.; Laser Flash Photolysis and Computational Studies of Ortho-Substituted Arylnitrenes, Arylchlorocarbenes, and Triplet Riboflavin Tetraacetate. *The Ohio State University,* **2003**.

19. Das, P. K.; Deslauriers, P. J.; Fahey, D. R.; Wood, F. K.; Cornforth, F. J. Photodegradation and Photostabilization of Poly(p-phenylene sulfide).1. Laser Flash Photolysis Studies of Model Compounds. *Macromolecules*. **1993,** *26*, (19), 5024-5029.

20. Yuan, H. X.; Wu, Y. L.; Zhao, J. F.; Dong, W. B. Laser Flash Photolysis Mechanism of Pyrenetetrasulfonate in Aqueous Solution. *Acta Phys-Chim. Sin*. **2012,** *28*, (4), 957-962.

21. Sanjuán, A.; Aguirre, G.; Alvaro, M.; Garcia, H.; Scaiano, J.C. Degradation of Propoxur in Water Using 2,4,6-triphenylpyrylium–Zeolite Y as Photocatalyst Product Study and Laser Flash Photolysis. *Appl Catal B-Environ*. **2000,** *25*, 257–265.

22. Sun, X.; Zhang, C.; Zhao, Y.; Bai, J.; Zhang, Q.; Wang, W. Atmospheric Chemical Reactions of 2,3,7,8-tetrachlorinated Dibenzofuran Initiated by An OH Radical: Mechanism and Kinetics Study. *Environ. Sci. Technol*. **2012,** *46*, (15), 8148-8155.

23. Atifi, A.; Talipov, M.; Mountacer, H.; Ryan, M. D.; Sarakha, M. A Density Functional Theory and Laser Flash Photolysis Investigation of Carbofuran Photodegradation in Aqueous Medium. *J Photoch Photobio A*. **2012,** *235*, 1-6.

24. Padmanabhan, J.; Parthasarathi, R.; Subramanian, V.; Chattaraj, P. K. Chemical Reactivity Analysis on 33′ 44′ 55′ -hexa Chlorobiphenyl—A DFT Approach. *Journal of Molecular Structure: THEOCHEM*. **2005,** *730*, (1-3), 221-226.

25. Wang, S.; Hao, C.; Gao, Z.; Chen, J.; Qiu, J. Theoretical Investigation on Photodechlorination Mechanism of Polychlorinated Biphenyls. *Chemosphere*. **2014,** *95*, 200-5.

26. Krzeminska, A.; Paneth, P. DFT Studies of S_{N2} Dechlorination of Polychlorinated Biphenyls. *Environ. Sci. Technol*. **2016,** *50*, (12), 6293-8.

27. Dong, W. B.; Zhu, C. Z.; Fang, H. J.; OU, Y., B.; Zhang, R. X.; Hou, H. Q. Reaction Mechanism of the Nitrate Radical with Biphenyl in Acetonitrile.pdf. *Acta Chimica Sinica*. **2005,** *63*, (23), 2147-2152.

28. Roger, A.; Christopher, N. P.; William, P. L. C.; Arthur, M. W.; James, N. P. Jr. Kinetics of the Gas-Phase Reactions of NO_3 Radicals with A Series of Alkanes at 296 ± 2K. *J. Phys. Chem* **1984,** *88*, 2361-2364.

29. Baciocchi, E.; Giacco, T. D.; Sebastiani, G. V. Photochemical Oxidation and Autoxidation of Some Cycloalkanes Promoted by Ceric Ammonium Nitrate in Acetonitrile. *Tetrahedron Lett*. **1987,** *28*, (17), 1941-1944.

30. Glass, R. W.; Martin, T. W. Flash Generation and Decay Kinetics of the Nitrate Radical in Aqueous Nitric Acid Solutions. *J Am Chem Soc*. **1970,** *92*, (17), 5084-5093.

31. Wine, P. H.; Mauldin, R. L. III.; Thorn, R. P. Kinetics and Spectroscopy of the Nitrogen Oxide Radical NO_3 in Aqueous Ceric. *J. Phys. Chem*. **1988,** *92*, (5), 1156-1162.

32. Giacco, T. D.; E. Baciocchi, E.; Steenken, S. One-electron Oxidation of Alkylbenzenes in Acetonitrile by Photochemically Produced Nitrate Radical Evidence for An Inner-sphere Mechanism. *J. Phys. Chem*. **1993,** *97*, (21), 5451-5456

33. Baciocchi, E.; Rol, C.; Sebastiani, G. V.; Serena, B. Photochemical Nitrooxylation of Methylbenzenes by Cerium(IV) Ammonium-nitrate in Acetonitrile. *Tetrahedron Lett*. **1984,** *25*, (18), 1945-1946.

34. Osamu, I.; Seiji, A.; Masashi, I. Kinetic Study for Reactions of Nitrate Radical (NO,') with Substituted Toluenes in Acetonitrile Solution. *J. Org. Chem*. **1989,** *54*, (10), 2436-2441.

35. Sehested, K.; Hart, E. J. Formation and Decay of the Biphenyl Cation Radical in Aqueous Acidic

Solution. *J. Phys. Chem*. **1975,** *79*, (16), 1693-1696.

36. Frisch, M. J.; Trucks, G. W.; Schlegel, H. B.; Pople, J. A. Gaussian 09. *Gaussian, Inc.: Pittsburgh PA*. **2009**.

37. Caillie, C. V.; Amos, R. D. Geometric Derivatives of Density Functional Theory Excitation Energies Using Gradient-corrected Functionals. *Chem Phys Lett*. **2000,** *317*, 159-164.

38. Caillie, C. V.; Amos, R. D. Geometric Derivatives of Excitation Energies Using SCF and DFT. *Chem Phys Lett*. **1999,** *308*, 249-255.

39. Moller, C.; PLESSET, M. S. Note on an approximation treatment for many-electron systems. *Phys. Rev*. **1934,** *46*, 0618–0622.

40. Tomasi, J.; Mennucci, B.; Cances, E. The IEF Version of the PCM Solvation Method: an Overview of A New Method Addressed to Study Molecular Solutes at the QM Ab Initio Level. *J Mol Struc-Theochem*. **1999,** *464*, (1-3), 211-226.

41. Breneman, C. M.; Wiberg, K. B. Determining Atom-centered Monopoles from Molecular Electrostatic Potentials. the Need for High Sampling Density in Formamide Conformational Analysis. *J Comput Chem*. **1990,** *11*, (3), 361-373.

42. Reed, A. E.; Weinstock, R. B.; Weinhold, F. Natural Population Analysisa. *J Chem Phys*. **1985,** *83*, (2), 735.

43. Mulliken, R. S. Electronic Population Analysis on LCAO [Single Bond] MO Molecular Wave Functions. I. *J Chem Phys*.**1955,** *23*, (10), 1833.